Structure and Position of the N-Terminal Membrane-Binding Domain of pp60^{src} at the Membrane Interface†

Ken Victor and David S. Cafiso*

Department of Chemistry and Biophysics Program, University of Virginia, Charlottesville, Virginia 22901

Received August 28, 1997

ABSTRACT: Hydrophobic and electrostatic interactions between the acylated N-terminal end of Src and lipid bilayers are responsible for the attachment of this nonreceptor tyrosine kinase to the membrane−solution interface. To investigate the structure and dynamics of this domain at the membrane interface, a series of peptides based upon the N-terminal end of pp60^{src}, myr-src(2−16), was synthesized with single-site cysteine substitutions and derivatized with a sulfhydryl-reactive proxyl nitroxide. The EPR line shapes and mobility of these peptides when bound to the membrane interface were consistent with an extended peptide conformation, and no evidence was found for either a helical or sheet structure. Line shapes on the myristoylated N-terminal end indicate that this segment is more restricted in its motion than at the C-terminus. Although the membrane affinity of this peptide is much stronger in the presence of acidic lipid, EPR line shapes were not strongly affected by the presence of acidic lipid. An EPR power saturation technique was used to provide information on the position of nitroxides from the interface for the membrane-bound peptide. When membrane bound, labeled side chains at the N-terminal end of the peptide were found to lie in the aqueous phase near the membrane interface; however, for the C-terminal half of the peptide, residues were further off the membrane and were 10−15 Å from the interface. Peptides derived from the membrane and calmodulin binding domains of the myristoylated alanine-rich C kinase substrate and neuromodulin were previously found to be in extended conformations; however, side chains for these peptides penetrated the membrane−solution interface. We speculate that the relatively polar character of the N-terminal segment of Src and a Born repulsion energy prevent this peptide from penetrating into the membrane interface when membrane bound.

The Src family of nonreceptor tyrosine kinases is a critical group of enzymes that function in a broad range of cell-signaling events. For example, the Src tyrosine kinases play a role in the fibroblast's mitogenic response to growth factors (*1*−*4*), cytoskeletal rearrangements that result from thrombin and lysophosphatidic acid stimulation (*5*), and DNA synthesis that occurs in response to the colony stimulating factor-1 (*6*). The Src tyrosine kinases are also actively recruited to focal adhesion sites by binding to the newly phosphorylated focal adhesion kinase in response to integrin coupling to the extracellular matrix (*6, 7*).

The product of the cellular *src* gene, pp60^{c-src} (here referred to as Src),[1] is the prototypical example of this group of nonreceptor protein tyrosine kinases, which are active at the membrane interface. The membrane association of the Src protein as well as its corresponding oncoprotein homologue, the pp60^{v-src} protein of the Rous sarcoma virus (or v-Src), is mediated by its N-terminal domain. Both proteins have identical N-terminal binding sequences, and 80−90% of the protein is membrane-bound during steady-state conditions (*8, 9*). The importance of membrane binding is demonstrated by the fact that mutants of v-Src that fail to bind membranes retain tyrosine kinase activity but do not transform cells (*10, 11*). The N-terminal domain of Src is myristolyated and basic, and both these features enable the protein to reversibly bind membranes (*10*−*13*). The 14-carbon myristate of Src is cotranslationally coupled to the amino-terminal glycine residue by an amide bond, and the following 14 residues, which include three lysines, contain a net valence of +5 (Myr-GSSKSKPKDPSQRRR). The myristate tail interacts hydrophobically with the phospholipid membrane, and the energy of this interaction yields an association constant of $K_p^{myr} = 10^4\ M^{-1}$ (*14*). In addition, a positively charged peptide from the N-terminal domain of Src interacts electrostatically with the membranes containing acidic lipids, and this electrostatic interaction yields a binding constant of $K_p^{elec} = 10^3\ M^{-1}$ (*15*). Working in tandem, these two mechanisms account for the association constant, $K_p^{arc} = 10^7\ M^{-1}$, that is observed for a myristoylated Src-derived peptide in the presence of membranes containing acidic lipids (*15*−*17*).

† This work was supported by a grant from the National Science Foundation (MCB 9418318) and National Institutes of Health (GM 35215).

[1] Abbreviations: CD, circular dichroism; EPR, electron paramagnetic resonance; DCM, dichloromethane; DMF, dimethylformamide; HPLC, high-performance liquid chromatography; MALD TOF, matrix-assisted laser desorption time-of-flight; MARCKS, myristoylated alanine-rich C kinase substrate; MBHA, *p*-methylbenzhydrylamine; MOPS, morpholinopropanesulfonic acid; MTSSL, methanethiosulfonate spin label; NiEDDA, nickel ethylenediaminediacetic acid; myr-src(2−16), myristoylated N-terminal sequence of the pp60^{c-src} gene product; NM, neuromodulin; NMM, *N*-methylmorpholine; PC, phosphatidylcholine; PKC, protein kinase C; PS, phosphatidylserine; PyBOP, [(benzotriazolyl)oxy]tripyrrolidinophosphonium hexafluorophosphate; Src, pp60^{c-src}; TFA, trifluoroacetic acid; v-Src, pp60^{v-src}.

S0006-2960(97)02150-8 CCC: $15.00
Published on Web 02/13/1998

Scheme 1

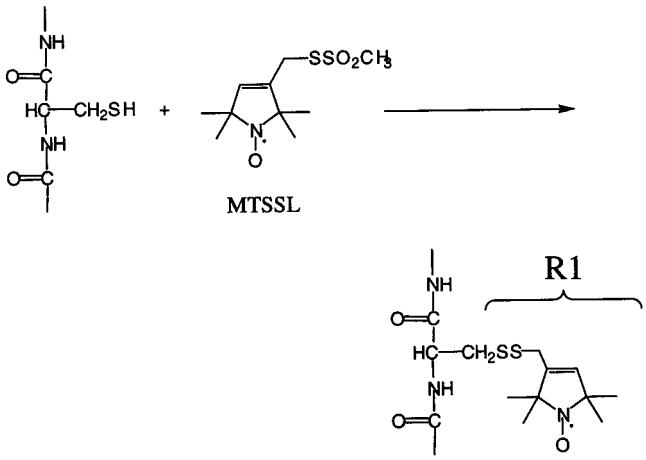

The use of acylation in tandem with an electrostatic interaction appears to be a general approach utilized by a variety of proteins to achieve membrane attachment. For example, the myristoylated alanine-rich C kinase substrate (MARCKS) resides in brain and several other tissues and is proposed to act as a PKC-regulated calmodulin buffer (*18*, *19*). In addition to its myristoylation, the MARCKS protein contains a highly basic, 25-amino acid domain, incorporating 12 lysines and one arginine residue, which electrostatically associates with negatively charged membranes (*20*). Phosphorylation of MARCKS results in its membrane dissociation, and this event functions as an electrostatic "switch" that can be used to control the membrane association of the protein (*16*).

Recent studies utilizing a continuous wave EPR power saturation technique have helped characterize the membrane-bound structures of peptides based on the positively charged effector domains of MARCKS and neuromodulin (NM) (*21*, *22*). The results of these studies indicate that the position and dynamics of these domains with respect to the water−membrane interface depend on the valence of the peptide and the presence of residues with hydrophobic side chains, as well as the charge density of the lipid membrane (*21*, *22*). The location of the these peptides along the bilayer normal likely reflects a balance between attractive and repulsive forces, where the attractive forces include a Coulombic attraction and the hydrophobic effect and the repulsive forces include the Born repulsion (*23*). The basic domains of Src, MARCKS, and neuromodulin also contain one or more PKC phosphorylation sites, and the balance of these forces may influence the accessibility of these substrates to PKC.

In the present report, the membrane-bound structure and dynamics of the N-terminal binding domain of Src, myr-src(2−16), are examined. This portion of the protein was not included in the crystal structure recently reported for the Src tyrosine kinase (*24*). Peptides are synthesized with a single cysteine substitution and derivatized with the SH-specific methanethiosulfonate spin label shown in Scheme 1 to produce a peptide with the side chain R1. Conventional cw EPR spectroscopy combined with power saturation is then used to examine the structure, dynamics, and position of the peptide bound to the membrane−solution interface.

EXPERIMENTAL PROCEDURES

Materials. Egg phosphatidylcholine (PC), bovine brain phosphatidylserine (PS), headgroup spin-labeled PC, and spin-labeled doxylphosphatidylcholines [1-palmitoyl-2-stearoyl(*n*-doxyl)phosphatidylcholines, $n = 5, 7, 10, 12$] were obtained from Avanti Polar Lipids (Alabaster, AL) and used without further purification. The methanethiosulfonate spin label, *S*-(1-oxy-2,2,5,6-tetramethylpyrroline-3-methyl) (MTSSL), was purchased from Reanal (Budapest, Hungary). Nickel ethylenediaminediacetic acid (NiEDDA) was synthesized by following a protocol that was provided by Dr. Christian Altenbach. [(Benzotriazolyl)oxy]tripyrrolidinophosphonium hexafluorophosphate (PyBOP) and all N^{α}-Fmoc L-amino acids were purchased from Novabiochem (La Jolla, CA). *N*-Methylmorpholine (NMM), piperidine, and pyridine were obtained from Aldrich Chemical Co. (Milwaukee, WI). Peptide synthesis grade dichloromethane (DCM) and dimethylformamide (DMF) were obtained from Fisher Scientific (Pittsburgh, PA). Trifluoroacetic acid (TFA) was purchased from Applied Biosystems (Foster City, CA), and acetonitrile was obtained from Mallickrodt Chemicals (Chesterfield, MO).

Peptide Synthesis. A series of 10 single-site mutants of a 15-residue peptide that corresponds to the N-terminus of the Src, myr-src(2−16), were synthesized on a Gilson automated multiple peptide system (AMS 422) using a rink amide *p*-methylbenzhydrylamine (MBHA) resin. These 10 mutants contained a single cysteine substituted at peptide residue positions 1, 3−5, and 9−14. Once the synthesis was complete, the dried resin wafers were swollen with pyridine and then washed repeatedly with DMF. A 3 times molar excess of myristic anhydride, dissolved in a solution containing 77% DMF and 23% pyridine, was then added to each resin wafer to alkylate the N-terminus of the nascent peptides. Next, a solution of 89% trifluoroacetic acid, 3% thioanisole, 2% anisol, 3% dithioethanol, and 3% water was employed as a cleavage bath for 5 h at room temperature to separate the myristoylated peptides from the resin. A cold ether bath precipitated these peptides which were then lyophilized and redissolved several times in water. The myristoylated peptides were spin-labeled by dissolving a 3 times molar excess of the sulfhydryl-reactive MTSSL in acetonitrile and then mixing this solution with the myristoylated peptide suspended in water. This spin label derivatization was allowed to react for several hours in the dark at room temperature. Finally, the spin-labeled peptides were purified on a Poros perfusion reversed-phase high-performance liquid chromatography (HPLC) column (PerSeptive Biosystems, Cambridge, MA) using a water−acetonitrile elution system. The gradient of the solvents used for the purification depended upon the particular peptide, but typically the acetonitrile was varied from 0% to 65% over 15 min. No TFA was added to the elution solvents because initial results indicated that the acid was breaking the peptides at the proline residue. Once purified, the identity of the synthetic peptide was confirmed by MALD TOF mass spectrometry.

Lipid Vesicle Preparation. Lipid mixtures containing the desired mole ratio of phosphatidylcholine (PC) and phosphatidylserine (PS) were created from stock lipid solutions of predetermined concentration in chloroform. After the chloroform was completely removed by an overnight vacuum

desiccation, the dried lipid mixture was resolvated by the addition of a pH 7.0 buffer containing 100 mM KCL and 10 mM MOPS. Unilamellar vesicles were produced by freeze−thawing this suspension five times using liquid nitrogen and then extruding the mixture through 0.1-μm pore diameter polycarbonate filters (Poretics, Livermore, CA) using a LiposoFast extruder (Avestine, Ottawa, Canada). For the EPR power saturation measurements, stock lipid solutions contained a 125 mM total lipid concentration, while 10 mM stock solutions were produced for the lipid titration measurements.

Measuring Partition Coefficients. The membrane binding affinity of spin-labeled myr-src(2−16) was determined using an EPR technique described previously (*25*). Briefly, the peak-to-peak amplitude of the $m_i = -1$ resonance of the nitroxide-spin-labeled peptide was measured as a function of the concentration of lipid. For vesicles containing only PC, an X-band loop−gap resonator with a standard two-loop, one-gap configuration was used to make the binding measurement. Lipid titration measurements with PC:PS (5:1) acidic vesicles required a lower peptide concentration, because of the enhanced membrane binding of the peptide, and in this case a rectangular cavity holding a 250-μL flat quartz cell was employed. The peptide signal was titrated with lipid until the EPR spectrum indicated that the peptide was fully bound to lipid. For each spectrum taken during the lipid titration, the mole ratio of membrane bound to aqueous peptide, λ, was calculated as described previously (*26*). The partition coefficient with units of length, β, was determined by assuming that the binding behavior of the peptide could be described by:

$$\frac{1}{C_L} = \beta A_L \frac{1}{\lambda} + V_L \qquad (1)$$

where C_L is the lipid concentration, A_L is the area per lipid, and V_L is the volume per mole of lipid. The values of 66 Å^2 and 1255 Å^3 for A_L and V_L, respectively, were employed (*27*). The molar partition coefficient used previously, K_1 in units of M^{-1}, is equivalent to $2\beta A_L$ (*15*).

EPR cw Power Saturation Measurements. Continuous-wave power saturation measurements were made on a Bruker ESP 300 spectrometer using an a X-band loop−gap resonator (Medical Advances, Milwaukee, WI). The samples contained 100 μM peptide in the presence of lipid vesicles at a total phospholipid concentration of 100 mM. At these concentrations, the peptide was fully bound to the lipid. The samples were held within the EPR resonator by gas-permeable TPX capillaries (Medical Advances, Milwaukee, WI). The microwave power was varied from roughly 0.24 to 200 mW, with the exact range depending upon the particular peptide being examined. For each power setting, the peak-to-peak amplitude of the $m_i = 0$ resonance, A, of the nitroxide spin-labeled peptide was measured. The dependency of A on the incident microwave power, P, can be expressed as follows:

$$A = I\sqrt{P}\left[1 + (2^{1/\epsilon} - 1)\frac{P}{P_{1/2}}\right]^{-\epsilon} \qquad (2)$$

where I is a scaling factor, $P_{1/2}$ is the microwave power required to reduce the resonance amplitude to one-half its unsaturated value, and ϵ is a measure of the homogeneity of the saturation of the resonance (*28*). By allowing I, ϵ, and $P_{1/2}$ to be adjustable parameters in a fit of the data to eq 2, a characteristic $P_{1/2}$ is obtained. Values for $P_{1/2}$ are then generated for each sample under three different sets of conditions: (1) equilibrated with a N_2, (2) equilibrated with air (20% O_2), and (3) equilibrated with N_2 in the presence of 20 mM NiEDDA. A depth parameter, Φ, is then calculated from the three $P_{1/2}$ values as follows:

$$\Phi \equiv \ln\left[\frac{P_{1/2}(O_2) - P_{1/2}(N_2)}{P_{1/2}(\text{NiEDDA}) - P_{1/2}(N_2)}\right] \equiv \ln\left[\frac{\Delta P_{1/2}(O_2)}{\Delta P_{1/2}(\text{NiEDDA})}\right] \qquad (3)$$

Since Φ is directly related to the difference in the standard state chemical potentials of O_2 and NiEDDA and varies as a function of depth in the lipid bilayer, Φ provides an estimate of the relative nitroxide depth in the lipid bilayer (*28*).

Calibration curves were obtained with the same lipid compositions used for measurements on myr-src(2−16) in order to convert Φ values into an absolute distance with respect to the membrane surface. Each calibration curve was obtained by employing a series of nitroxide-labeled PCs: a headgroup spin-labeled PC and spin-labeled PCs with doxyl nitroxides at positions 5, 7, and 10 along the alkyl chain. While still suspended in chloroform, these spin-labeled lipids were codissolved with the desired mixture of nonlabeled lipids. This composite lipid mixture was then dried, hydrated, and extruded to form vesicles as described above. The EPR power saturation measurements, obtained in the absence of all peptides, were made with a total lipid concentration of 100 mM and a spin-labeled lipid concentration of 250 μM.

RESULTS

Membrane Partitioning and Dynamics of the pp60^{src} Peptide. Shown in Figure 1 are the EPR spectra of two single-site cysteine-substituted mutants of mry-src(2−16) as a function of increasing lipid concentration. The left-hand side of this figure contains spectra of the S4C-SL mutant as it is titrated with PC lipid vesicles, while the right-hand side contains spectra of the P11C-SL mutant being titrated with PC:PS (5:1) lipid vesicles. The EPR spectra for these peptides freely diffusing in solution are similar to the spectra found for other labeled peptides in aqueous solution (*21*, *22*, *29*). A low-amplitude broad component seen in the spectra for P11C-SL is due to the binding of the peptide to the quartz EPR cell.[2] The introduction of lipid significantly alters the

[2] A slow motional component is seen for the spin-labeled Src peptide P11C-SL in Figure 1 even when no lipid is present. This signal, which is apparent throughout this titration, is a result of the binding of this peptide to the EPR quartz cell surface. The strength of this component quickly saturates and is seen only at the low concentrations necessary for titration to PC:PS membranes. This signal is obscured at higher spin concentrations such as those used in the titration of S4C-SL to PC membranes. The EPR sample cell can be rinsed several times with buffer, and the bound component persists. The dissociation of this peptide from the glass is apparently very slow on the time scale of our experiments, and as a result, its binding to quartz should not affect the determination of the membrane partition coefficient.

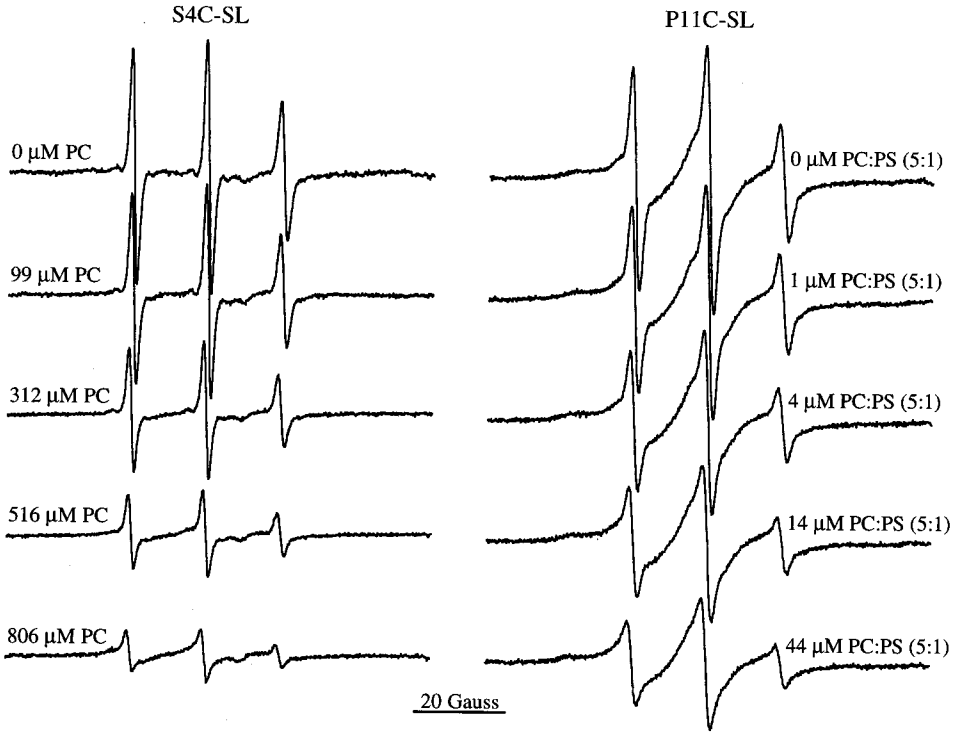

FIGURE 1: EPR spectra of the myr-src(2−16) mutants S4C-SL and P11C-SL. The S4C-SL peptide, its concentration ranging from 100 to 87 μM, is titrated with lipid vesicles composed of only PC. The P11C-SL peptide at 8 μM is titrated with vesicles composed of PC:PS (5:1). All of the lipid vesicles were 100 nm in diameter, the pH = 7 buffer contained 100 mM KCl and 10 mM MOPS, and all the spectra were taken at 25 °C with a scan width of 100 G for 480 s. For P11C-SL, the broad immobile component that can be seen even in the absence of lipid is a result of the binding of this peptide to the quartz flat cell. This broad component is only seen when the concentrations of free peptide are low.

EPR spectra of the peptides, gradually broadening and decreasing the amplitude of the resonances. From the amplitude of the high-field resonance, the bound-to-free peptide ratio is determined as a function of lipid concentration, and these data are plotted in Figure 2. The molar partition coefficient, K_1, was determined as described above from the data in Figure 2 and yielded a value of 4.4×10^3 M^{-1} for the peptide S4C-SL in PC and a value of 6.4×10^5 M^{-1} for the peptide P11C-SL in PC:PS (5:1) containing membranes. From the binding of several peptides, we obtained averaged values for K_1 of 4.6×10^3 M^{-1} to PC vesicles and of 8.9×10^5 M^{-1} to PC:PS vesicles. These partition coefficients are similar to those found previously (*15*) and indicate that the substitution of these residues with the nitroxide side chain does not significantly alter the energetics of the peptide−membrane interaction.

Shown in Figure 3 are the EPR spectra of the 10 spin-labeled derivatives of myr-src(2−16) at a lipid concentration sufficiently high so that the peptides are completely associated to PC:PS (3:1) membranes. A comparison of these spectra reveals several notable features. First, the peptide side chains become increasingly more mobile as one moves from the N- to the C-terminus. An examination of the high-field resonance clearly illustrates this trend as the resonance narrows and increases in amplitude as one moves toward the C-terminus. The line shapes at the N-terminus from residues 2−6 are similar to those obtained previously for the extended peptide MARCKS(151−175) bound to the membrane interface. However, the spectra obtained for residues 12−15 are considerably more mobile than we have seen for other membrane-associated peptides and resemble the spectra obtained at the N-terminus of MARCKS(151−175) which is extended from the membrane interface (*22*). In Figure 3, the spectrum for R15C-SL appears to be a composite of more than one motional component. This may be a result of two or more slowly converting configurations for the spin-labeled side chain, R1, or two or more

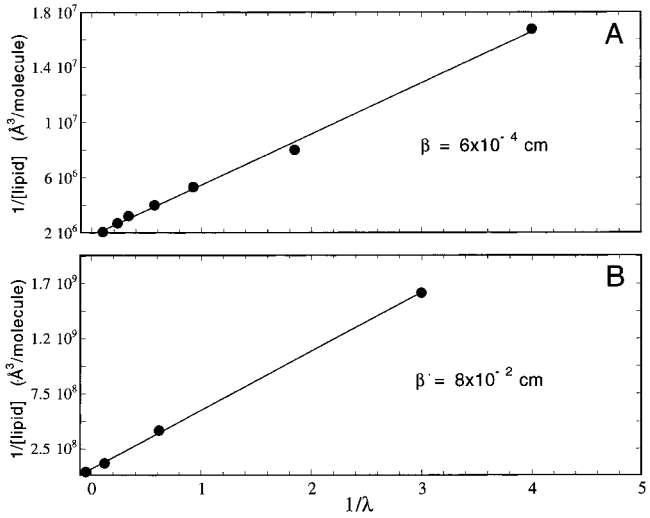

FIGURE 2: Measurement of the partition coefficient, β, for (A) S4C-SL and (B) P11C-SL, based upon the lipid titrations illustrated and described in Figure 1. The solid lines represent fits to the data (●) using eq 1, where A_L was assumed to be 66 Å^2, and yield values of β of 6×10^{-4} and 8×10^{-2} cm, respectively (*27*). The molar partition coefficient for binding to PC was determined for G2C-SL, S4C-SL, K5C-SL, and S6C-SL and yielded values of 5.4×10^3, 4.4×10^3, 4.0×10^3, and 1.8×10^3 M^{-1}, respectively. The molar partition coefficient for binding to PC:PS (5:1) was determined for S6C-SL and P11C-SL and yielded values of 11.4×10^5 and 6.4×10^5 M^{-1}, respectively.

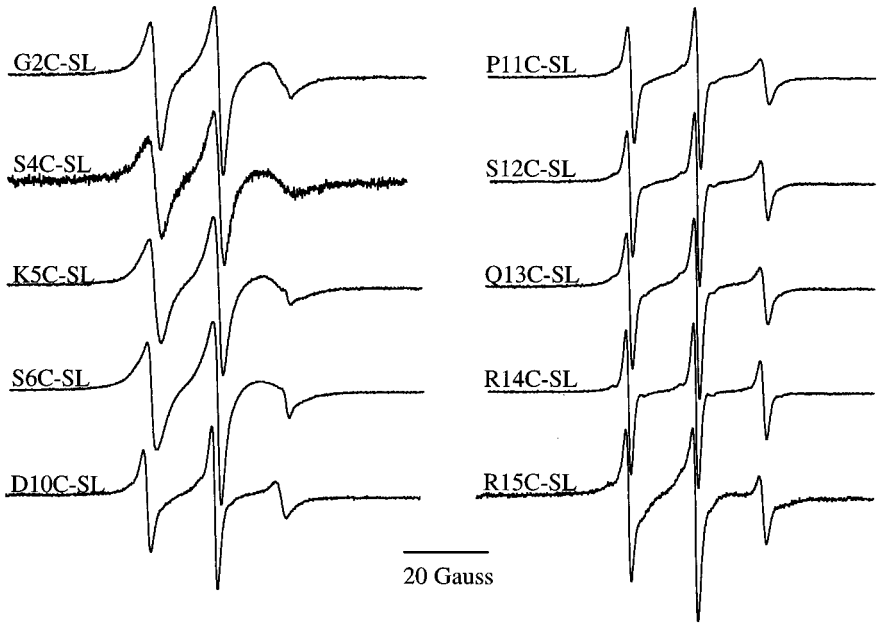

FIGURE 3: EPR spectra of the myr-src(2−16) mutants fully bound to 100-nm (diameter) PC:PS (3:1) lipid vesicles. The lipid concentration of 100 mM is at least 1 order of magnitude higher than is necessary to completely bind the peptides (100 μM) (see Figure 1). The pH = 7 buffer contained 100 mM KCl and 10 mM MOPS, and all the spectra were taken at 25 °C with a scan width of 100 G for 336 s.

Table 1: Values for $\Delta P_{1/2}$, Φ, Rotational Correlation Time, τ_c, and Averaged Hyperfine Coupling Constant (A_o) for Spin-Labeled pp60^{src} Peptides Fully Bound to 100-nm Diameter Lipid Vesicles Composed of PC:PS (3:1)

peptide	$\Delta P_{1/2}$(air)[a]	$\Delta P_{1/2}$(NiEDDA)[a]	Φ	τ_c (ns)	A_o(G)
G2C-SL	11.0	3.7	1.1	1.7	14.8
S4C-SL	9.6	3.9	0.9	2.1	15.2
K5C-SL	11.1	3.1	1.3	2.1	14.9
S6C-SL	9.3	5.5	0.5	1.7	15.9
D10C-SL	5.5	12.1	−0.8	1.0	16.0
P11C-SL	4.1	41.0	−2.3	0.8	16.1
S12C-SL	3.6	39.4	−2.4	0.6	16.1
Q13C-SL	4.1	37.2	−2.2	0.7	16.1
R14C-SL	4.5	36.4	−2.1	0.4	16.2
R15C-SL	5.3	8.4	−0.5	0.7	16.1

[a] Values for $\Delta P_{1/2}$ are given in mW. Air contains approximately 20% O_2 which is a hydrophobic paramagnetic species. NiEDDA, an uncharged hydrophilic paramagnetic species, was added to a final concentration of 20 mM.

configurations for this end of the peptide.

Shown in Table 1 are the averaged hyperfine splittings (A_o) measured from the spectra of Figure 3, a spectral parameter that is sensitive to the polarity of the environment (*30*), and the rotational correlation time, τ_c, for the R1 side chains.[3] These data indicate that the C-terminus of the peptide myr-src(2−16) resides in a more polar environment than its N-terminus, and the averaged hyperfine splittings for the C-terminal half of myr-src(2−16) are virtually identical whether the peptide is fully bound to the membrane or freely diffusing in solution without lipids present. The correlation times, τ_c, decrease from the N- to the C-terminus. At the N-terminus, these rates are consistent with those found previously for membrane-associated peptides, while at the C-terminus the motional rates are close to those found for peptides in solution. For surface-exposed residues on a protein, the dynamics of the nitroxide side chain R1 have been shown to reflect backbone dynamics (*31*). As a result, the differences seen between the N- and C-terminal domains of myr-src(2−16) are likely to reflect differences in backbone dynamics on the nanosecond time scale.

In Figure 4, a comparison of the line shapes for myr-src-(2−16) bound to either PC or PC:PS is shown. The spectra for the labeled peptides fully bound to PC lipid vesicles follow the same general trends discussed above for the PC:PS (3:1) vesicles. In fact, the most remarkable feature in this comparison is the similarity between the spectra of each mutant when it is fully bound to either PC or PC:PS (3:1) lipid vesicles. This similarity is also reflected in the agreement between the hyperfine splittings for the peptides bound to the PC vesicles, listed in Table 2, and bound to PC:PS, listed in Table 1. These results suggest that while acidic phospholipids strongly enhance the membrane partitioning of the Src peptide, they do not significantly change the dynamics or structure of the peptide when bound to the membrane interface.

Membrane-Bound Position of the pp60^{src} Peptide. Previous work has demonstrated that EPR power saturation in the presence of hydrophobic and aqueous paramagnetic species can be used to determine the position of a nitroxide along the membrane normal (*21*, *22*, *28*, *32*). This approach was used here to examine the position of the nitroxide side chains from the membrane−solution interface for membrane-bound myr-src(2−16). Shown in Figure 5 is an example of a power saturation curve for the membrane-bound nitroxide-labeled peptide D10C-SL. The decrease in the initial slope of the curves obtained in the presence of air (20% O_2) and NiEDDA compared to that obtained in the presence of N_2 indicates that more microwave power is necessary to saturate the EPR signal of the peptide-bound nitroxide. This difference is a result of the collisional frequency between the

[3] The rotational correlation times calculated here and shown in Tables 1 and 2 are rigorously correct only for a label having isotropic motion. Since the labeled peptides clearly exhibit anisotropic motion, these estimated correlation times are approximate and are intended only to provide a comparison of the rates of motion between different segments of the peptide.

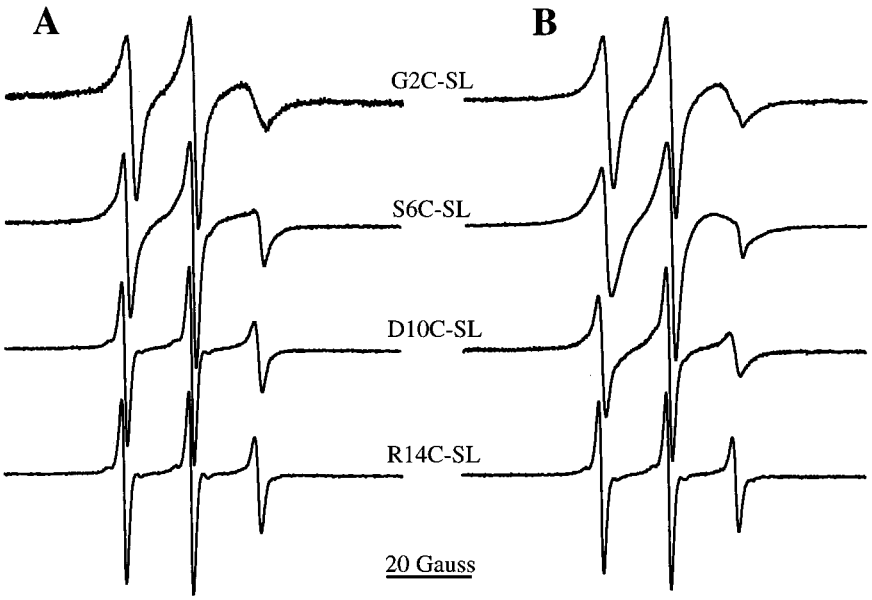

FIGURE 4: EPR spectra of four of the myr-src(2−16) mutants fully bound to both (A) PC and (B) PC:PS (3:1) lipid vesicles. The conditions are the same as those described for Figure 5.

Table 2: Values for $\Delta P_{1/2}$, Φ, Rotational Correlation Time, τ_c, and Averaged Hyperfine Coupling Constant (A_o) for Spin-Labeled pp60^{src} Peptides Fully Bound to 100-nm Diameter Lipid Vesicles Composed of Only PC

peptide	$\Delta P_{1/2}$(air)[a]	$\Delta P_{1/2}$(NiEDDA)[a]	Φ	$\tau_{c\ (ns)}$	A_o (G)
G2C-SL	10.1	1.3	2.1	1.6	14.8
S6C-SL	5.6	8.7	−0.4	1.0	16.0
D10C-SL	3.8	46.4	−2.5	0.6	16.1
R14C-SL	3.3	47.4	−2.7	0.4	16.2

[a] Values for $\Delta P_{1/2}$ are given in mW. Air contains approximately 20% O_2 which is a hydrophobic paramagnetic species. NiEDDA, an uncharged hydrophilic paramagnetic species, was added to a final concentration of 20 mM.

nitroxide and each paramagnetic reagent. The lines in Figure 5 represent fits of the data to eq 2 and were used to obtain values for $P_{1/2}$. These data were then used to determine the values of $\Delta P_{1/2}$ and the depth parameter Φ as defined in eq 3. The values of $\Delta P_{1/2}$ and Φ for the 10 spin-labeled derivatives of myr-src(2−16) are shown in Table 1.

Shown in Table 2 are values of $\Delta P_{1/2}$ in the presence of O_2 (air) and NiEDDA and the value of Φ for four of the peptides derived from mry-src(2−16) bound to PC in the absence of acidic lipid. The data indicate that the C-terminus of myr-src(2−16) is more accessible to NiEDDA and less accessible to O_2 (air) than its N-terminus regardless of the lipid vesicle system. The region of transition is roughly centered about the tenth residue (D10C-SL). The Φ values illustrate the same trend and are directly related to the standard state chemical potential difference between the paramagnetic agents at a particular position with respect to the water−membrane interface (*28*). Measurements for the unbound peptides in the absence of lipid all yielded values for Φ that were approximately −2.3. These results are qualitatively consistent with those suggested by the hyperfine splittings (A_o).

To assign a depth to the values of Φ listed in Tables 1 and 2, Φ was calibrated as a function of distance from the membrane interface for the experimental conditions and phospholipid compositions used here. The calibration was

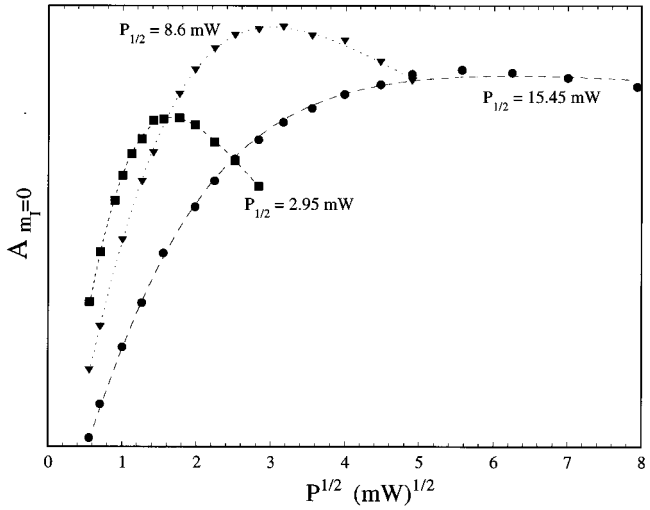

FIGURE 5: Power saturation curves obtained for the D10C-SL mutant of the pp60^{src} peptide while fully bound to 100-nm (diameter) PC:PS (3:1) lipid vesicles. The pH = 7 buffer contained 100 mM KCl and 10 mM MOPS, and all the spectra were taken at 25 °C. Amplitudes of the $m_i = 0$ line in the absence of any paramagnetic reagent (■), in the presence of air (▼), and in the presence of 20 mM NiEDDA (●) are illustrated as functions of the square root of the microwave power ($P^{1/2}$). The dashed lines denote the curve fit to the data using eq 2. The listed $P_{1/2}$ values were extracted from the curve fit and used to calculate the corresponding Φ parameter (see Table 1).

obtained by conducting EPR power saturation measurements on lipid vesicles that contained 0.25 mol % nitroxide-labeled lipids. Shown in Figure 6 are the values of Φ obtained for both PC and a PC:PS (3:1) lipid vesicle system as a function of distance from the phosphate group for a series of spin-labeled lipids (*33*, *34*). As shown previously, the data yield an approximately linear behavior of Φ as a function of position from the lipid phosphate. The *n*-doxyl PCs labeled at $n = 12$ and 16 were not used in determining the calibration curve shown here, because the gradient of NiEDDA at the concentrations used here is too small to permit accurate measurements of $\Delta P_{1/2}$. In addition, the 16-doxyl PC position was shown previously to be distorted because of

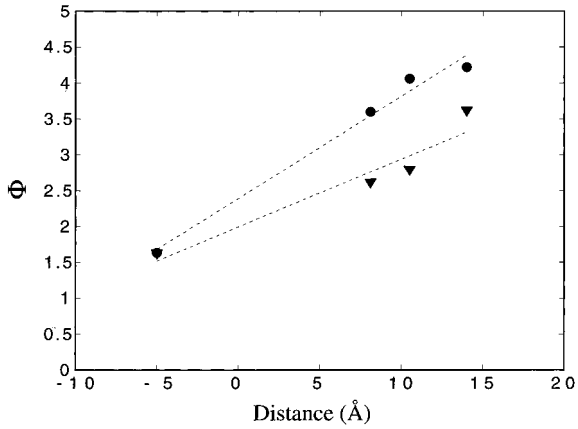

FIGURE 6: Depth calibration for the value of Φ. Values of Φ were calculated using eq 3 and are plotted versus the distance of the nitroxide from the phosphate group. Values for the depths of the *n*-doxyl PCs with $n = 5$, 7, and 10 were obtained using previously reported values (*33*). The headgroup-labeled PC (Tempo-PC) was assigned to a position of −5 Å (*34*). The calibration was conducted for vesicles composed of both PC (●) and PC:PS (3:1) (▼). The dashed lines represent the best fit and were used to estimate distances from the measured Φ values of the membrane-bound Src peptides.

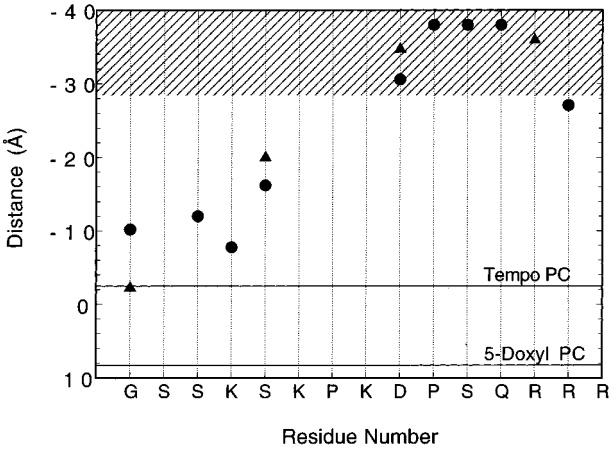

FIGURE 7: Nitroxide distances from the phosphate group at the membrane−solution interface as a function of the residue position on myr-src(2−16). The distances are calculated from the measured Φ values for mutant Src peptides that are shown in Tables 1 and 2 using the calibration curves in Figure 6. The nitroxide positions are shown for the peptide fully bound to PC (●) and PC:PS (3:1) (▲) lipid vesicles. The shaded regions at the top of the graph indicate distances that cannot be accurately distinguished because Φ values are within experimental error of the Φ values observed for aqueous peptides in the absence of lipid (see text).

the dynamics of the acyl chain terminus (*28*).

The distance data shown in Figure 7 were obtained from the values of Φ for the spin-labeled myr-src(2−16) peptides using the calibration shown in Figure 6. The distances demonstrate that the spin label R1 side chains for the membrane-bound peptide lie in the aqueous phase with the side chains at the N-terminus lying closer to the lipid phosphate than side chains at the C-terminus. The myristoylation apparently anchors the N-terminus closer to the membrane. The last labeled residue at the C-terminus appears to twist back slightly toward the membrane interface, a feature that is also reflected in the values of *A*o (see Table 1).

Distances for side chains that are far away from the membrane interface in Figure 7 (greater than 10−15 Å) must be viewed with some caution. The concentration gradient of either paramagnetic agent will be small at distances removed more than 10−15 Å from the interface; hence, there will be a significant amount of error in estimating distances even though the measurement of Φ is highly reproducible. Indeed, on the C-terminal half of the peptide, many of the residues exhibit an accessibility to paramagnetic agents that is indistinguishable from that obtained in a bulk aqueous phase; thus there is no difference in the local concentration of O_2 or NiEDDA to discriminate the position of R1. Furthermore, the calibration curve shown in Figure 6 was generated from a set of standard nitroxide-labeled lipids where no distances were greater than 5 Å above the level of the lipid phosphate. Estimated distances near −5 Å are expected to be reasonably accurate; however, distances that are much further out assume a linear behavior that may not hold further out into the aqueous phase.

Despite the above limitations, the calibrated distances provide useful information about the membrane-bound structure of myr-src(2−16). Note that the presence of acidic phospholipids in the bilayer does not significantly alter the position of the peptide. This is particularly surprising because the C-terminus of myr-src(2−16) ends with three positively charged arginine residues. Also note that it is in the region containing the three positively charged lysine residues that the peptide begins to position itself further away from the water−membrane interface.

Conformation of the Membrane-Bound Src (1−15). The myristoylated peptide Src(1−15) appears to be in an extended structure on the membrane interface. There is no indication from either the EPR line widths, hyperfine couplings, or depth parameters for a helical or sheet structure on the membrane interface. The EPR line widths indicate that the peptides are monomeric and not aggregated on the membrane interface. Furthermore, the central line width (ΔH_o) and the second moments of the EPR spectra are consistent with attachment of the nitroxide side chain, R1, to a highly flexible structure (*31*).

DISCUSSION

The EPR results obtained here lead to several significant conclusions regarding the structure of myr-src(2−16) on the membrane surface. First, the membrane-bound peptide lies on the aqueous side of the membrane−solution interface. This result is consistent with surface pressure measurements, which indicate that nonmyristoylated peptides derived from the N-terminus of Src do not penetrate the membrane interface (S. McLaughlin, personal communication). Second, the peptide is in an extended conformation, and there is no indication for a regular helical or sheet structure. These data is consistent with CD data that were obtained previously for Src-derived peptides (*15*). The lack of a secondary structure for basic membrane-binding peptides is not unexpected. Extended structures were previously found using site-directed spin labeling and EPR for peptides derived from the basic membrane-binding protein domains of MARCKS and neuromodulin (*21, 22*). The EPR results also indicate that the dynamics of the peptide backbone and side chain increase from the N- to the C-terminal end of the peptide, with the C-terminus lying further off the membrane surface than the myristoylated end of the peptide.

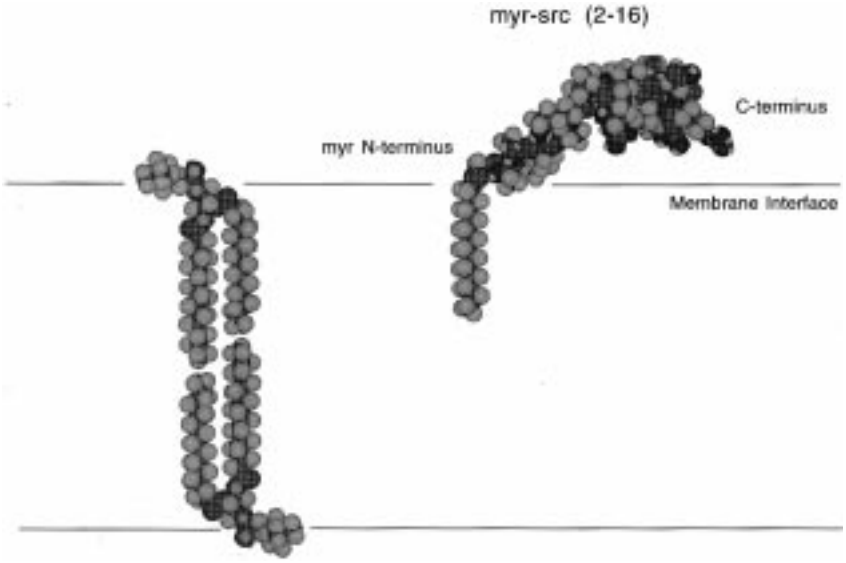

FIGURE 8: One of several likely configurations for the peptide myr-src(2−16) based on the EPR data obtained here and other energetic considerations. In this configuration, the charged side chains at the C-terminus are approximately 7−8 Å from the membrane interface. A neutral side chain such as R1 in some portions of the C-terminus could lie as much as 20 Å from the interface, while groups at the N-terminus are restricted to lie near the interface.

In comparison to MARCKS(151−175) and NM(37−53), the side chains for myr-src(2−16) assume a dramatically different position relative to the membrane interface. When derivatized to either the MARCKS- or the NM-derived peptides, the R1 side chain assumes a position that is buried within the membrane−solution interface. For MARCKS-(151−175) the EPR data are consistent with surface pressure measurements (*35*) and suggest that the five phenylalanines of this domain are inserted into the interfacial region of the lipid bilayer. For highly charged basic peptides such as pentalysine (Lys_5), the position of the peptide on the membrane interface is expected to be determined in part by the balance of a long-range Coulombic attraction and a short-range Born repulsion (*23*). Peptides such as Lys_5 do not contact or penetrate the membrane−solution interface apparently because of the Born repulsion and because of a lack of hydrophobic side chains (*23, 36, 37*). MARCKS(151−175) and NM(37−53) contain a number of hydrophobic side chains, and apparently the hydrophobic binding energy of these side chains allows these peptides to overcome the Born repulsion and approach the membrane interface. Despite its N-terminal myristoylation, myr-src(2−16) is a rather polar peptide as judged from scales that measure the water−oil transfer free energy or more recent scales that measure the water−membrane interface transfer free energies (*38, 39*). As a result, it is not surprising that this Src-derived peptide behaves like Lys_5 rather than like MARCKS(151−175) or NM(37−53).

The spin-labeled peptide side chains of myr-src(2−16), particularly on the C-terminal half of the peptide, appear to reside some distance off the membrane interface, greater than 10−15 Å. As indicated below, this result is somewhat unexpected, and several points should be made regarding the interpretation of these data. First, it is important to note that the positions of the substituted R1 side chains may not reflect the positions taken by the charged Arg or Lys residues in myr-src(2−16). Second, as was noted above the furthest calibration point off the membrane interface for the depth parameter Φ, is only 5 Å from the interface. While distances within this calibration curve should be quite accurate (within 2−3 Å), the distances plotted in Figure 7 assume that the linear behavior of Φ is maintained at distances quite far from the interface. Since the validity of this assumption is currently not known, distances that are far from this surface may include a significant error. Experiments are currently underway using alternative approaches to map distances further from the interface to clarify these issues.

Several features of the interaction between charged peptides and membranes containing acidic lipids suggest that the charged residues must lie close to the surface. First, the Born repulsion is not expected to be significant until the peptide reaches within several angstroms of the membrane interface (*23*). Without additional forces acting to keep the peptide from the membrane interface, charged residues should reach an energy minimum near the interface. Second, if the charged side chains of this peptide resided far off the membrane interface (for example a Debye length or greater than 10 Å), they could not make a significant electrostatic contribution to the binding. Shown in Figure 8 is a CPK model and diagram indicating the relative position and structure of membrane-associated mry-src(2−16) based on the EPR data and the requirement that charged side chains reside close to the membrane interface. This peptide is clearly highly dynamic, and the diagram shown in Figure 8 represents one of many conformations that would be consistent with the available data. The charged side chains in Figure 8 are shown positioned near the membrane interface, with the C-terminus further off the surface on average than the myristoylated N-terminus. In this particular structure the charged side chains at the C-terminus can approach quite close to the membrane interface, while the uncharged R1 at some side-chain positions could be as much as 15−20 Å away. A final justification for the general features of the structure shown in Figure 8 is the fact that electrostatic calculations accurately predict the binding free energy of myr-src(2−16) when it assumes a configuration and position similar to that shown in Figure 8 (*40*).

In addition to the Born repulsion there are likely other nonelectrostatic forces acting to keep the C-terminus from approaching close to the interface. For example, a helical peptide that is bound to the membrane interface experiences a loss of one rotational and one translational degree of freedom, leading to an estimated free energy loss of 5 kcal/mol (*41*). The myr-src(2−16) is not helical, but the EPR spectra shown above indicate that the C-terminus is more dynamic and experiences more internal motion than the N-terminus, which is positioned near the interface. In fact, a remarkable feature of the EPR spectra for membrane-bound myr-src(2−16) is that spin labels at the C-terminus exhibit motion that is nearly identical to that for the unbound aqueous peptide, while the N-terminus shows a dramatic restriction in motion when membrane bound. The localization of the C-terminus further into the aqueous phase and its increased dynamics likely reflect the tendency of this end of the peptide to maximize its entropy. The more restricted dynamics of side chains at the N-terminus is likely a result of the interaction of its acyl chain with the membrane interface.

In summary, site-directed spin labeling and EPR spectroscopy have been used to examine the structure and position of the peptide myr-src(2−16) on the membrane interface. The peptide assumes an extended structure and lies on the aqueous side of the membrane−solution interface. The myristoylated N-terminus lies closer to the membrane interface and exhibits more restricted motion than at the peptide C-terminus. The aqueous location for this membrane-bound peptide is in contrast to that found for other membrane-binding basic protein domains and is likely a result of its relatively polar character.

ACKNOWLEDGMENT

We would like to thank Jaison Jacob for help in producing the molecular model shown in Figure 8. We would also like to thank Prof. Donald Hunt for the use of their multiple peptide synthesizer.

REFERENCES

1. Twamley-Stein, G. M., Pepperkok, R., Ansorge, W., and Courtneidge, S. A. (1993) *Proc. Natl. Acad. Sci. U.S.A. 90*, 7696−7700.
2. Wilson, L. K., Luttrell, D. K., Parsons, J. T., and Parsons, S. J. (1989) *Mol. Cell. Biol. 9*, 1536−1544.
3. Luttrell, D. K., Luttrell, L. M., and Parsons, S. J. (1988) *Mol. Cell. Biol. 8*, 497−501.
4. Roche, S., Koegl, M., Barone, M. V., Roussel, M. F., and Courtneidge, S. A. (1995) *Mol. Cell. Biol. 15*, 1102−1109.
5. Erpel, T., and Courtneidge, S. A. (1995) *Curr. Opin. Cell Biol.* 176−182.
6. Erpel, T., Superti-Furga, G., and Courtneidge, S. A. (1995) *EMBO J. 14*, 963−975.
7. Schlaepfer, D. D., Hanks, S. K., Hunter, T., and Geer, P. v. d. (1994) *Nature 372*, 786−791.
8. Courtneidge, S. A., Levinson, A. D., and Bishop, J. M. (1980) *Proc. Natl. Acad. Sci. U.S.A. 77*, 3783−3787.
9. Resh, M. D., and Erikson, R. L. (1985) *J. Cell. Biol. 100*, 409−417.
10. Cross, F. R., Garber, E. A., Pellman, D., and Hanafusa, H. (1984) *Mol. Cell. Biol. 4*, 1834−1842.
11. Kamps, M. P., Buss, J. E., and Sefton, B. M. (1985) *Proc. Natl. Acad. Sci. U.S.A.* 82, 4625−4628.
12. Resh, M. D. (1993) *Biochim. Biophys. Acta 1155*, 307−322.
13. Silverman, L., and Resh, M. D. (1992) *J. Cell. Biol. 119*, 415−425.
14. Peitzsch, R. M., and McLaughlin, S. (1993) *Biochemistry 32*, 10436−10443.
15. Buser, C. A., Sigal, C. T., Resh, M. D., and McLaughlin, S. (1994) *Biochemistry 33*, 13093−13101.
16. McLaughlin, S., and Aderem, A. (1995) *Trends Biochem. Sci. 20*, 272−276.
17. Sigal, C. T., Zhou, W., Buser, C. A., McLaughlin, S., and Resh, M. D. (1994) *Proc. Natl. Acad. Sci., U.S.A. 91*, 12253−12257.
18. McIlroy, B. K., Walters, J. D., Blackshear, P. J., and Johnson, J. D. (1991) *J. Biol. Chem. 266*, 4959−4964.
19. Taniguchi, H., and S. Manenti (1993) *J. Biol. Chem. 268*, 9960−9963.
20. Kim, J. K., Blackshear, P. J., Johnson, D. J., and McLaughlin, S. A. (1994) *Biophys. J. 67*, 227−237.
21. Wertz, S. L., Savino, Y., and Cafiso, D. S. (1996) *Biochemistry 35*, 11104−11112.
22. Qin, Z., and Cafiso, D. S. (1996) *Biochemistry 35*, 2917−2925.
23. Ben-Tal, N., Honig, B., Peitzsch, R. M., Denisov, G., and McLaughlin, S. (1996) *Biophys. J. 71*, 561−575.
24. Xu, W., Harrison, S. C., and Eck, M. J. (1997) *Nature 385*, 595−602.
25. Archer, S. J., Ellena, J. F., and Cafiso, D. S. (1991) *Biophys. J. 60*, 389−398.
26. Cafiso, D. S., and Hubbell, W. L. (1981) *Annu. Rev. Biophys. Bioeng. 10*, 217−244.
27. Flewelling, R. F., and Hubbell, W. L. (1986) *Biophys. J. 49*, 531−540.
28. Altenbach, C., Greenhalgh, D. A., Khorana, H. G., and Hubbell, W. L. (1994) *Proc. Natl. Acad. Sci. U.S.A. 91*, 1667−1671.
29. Altenbach, C. Froncisz, W., Hyde, J. S., and Hubbell, W. L. (1989) *Biophys. J. 56*, 1183−1191.
30. Seelig, J. (1970) *J. Am. Chem. Soc. 92*, 3881−3887.
31. Mchaourab, H., Lietzow, M., Hideg, K., and Hubbell, W. (1996) *Biochemistry 35*, 7692−7704.
32. Yu, Y. G., Thorgeirsson, T. E., and Shin, Y.-K. (1994) *Biochemistry 33*, 14221−14226.
33. Dalton, L. A., McIntyre, J. O., and Fleischer, S. (1987) *Biochemistry 26*, 2117−2130.
34. Farahbakhsh, Z. T., Altenbach, C., and Hubbell, W. L. (1992) *Photochem. Photobiol. 56*, 1019−1033.
35. Glaser, M., Wanaski, S., Buser, C. A., Boguslavsky, V., Rashidzada, W., Morris, A., Rebecchi, M., Scarlata, S. F., Runnels, L. W., Prestwich, G. D., Chen, J., Aderem, A., Ahn, J., and McLaughlin, S. (1996) *J. Biol. Chem. 271*, 26187−26193.
36. Roux, M., Neumann, J.-M., Bloom, M., and Devaux, P. F. (1988) *Eur. Biophys. J. 16*, 267−273.
37. Kim, J., Mosior, M., Chung, L. A., Wu, H., and McLaughlin, S. A. (1991) *Biophys. J. 60*, 135−148.
38. Engelman, D. M., Steitz, T. A., and Goldman, A. (1986) *Annu. Rev. Biophys. Biophys. Chem. 15*, 321−353.
39. Wimley, W. C., Creamer, T. P., and White, S. H. (1996) *Biochemistry 35*, 5109−5124.
40. Murray, D., Hermida-Matsumoto, L., Buser, C. A., Tsang, J., Sigal, C. T., Ben-Tal, N., Honig, B., Resh, M. D., and McLaughlin, S. A. (1998) *Biochemistry*, in press.
41. Ben-Tal, N., Ben-Shaul, A., Nicholls, A., and Honig, B. (1996) *Biophys. J. 70*, 1803−1812.

BI9721501